# First-principles growth kinetics and morphological evolution of Cu nanoscale particles in Al

Jianwei Wang [a], C. Wolverton [b], Stefan Müller [c], Zi-Kui Liu [a], Long-Qing Chen [a,*]

[a] *Department of Materials Science and Engineering, The Pennsylvania State University, University Park, PA 16802, USA*
[b] *Ford Research and Advanced Engineering, MD 3083/SRL, Dearborn, MI 48121-2053, USA*
[c] *Universität Erlangen-Nürnberg, Lehrstuhl für Festkörperphysik, Staudtstrasse 7, 91058 Erlangen, Germany*

## Abstract

The morphological evolution of nanoscale precipitates in Al–Cu alloys is studied by integrating first-principles calculations, the mixed-space cluster expansion, and Monte Carlo simulations. Without a priori assumptions, we predict generic precipitate morphologies dominated by strain-induced long-range interactions: single atomic layers consisting of 100%Cu atoms along {1 0 0} planes of a face-centered-cubic lattice of Al atoms, consistent with experimental measurements. We analyze the precipitation kinetics using the Johnson–Mehl–Avrami phase transformation theory and obtain a transformation exponent close to 1.5.
© 2005 Published by Elsevier Ltd on behalf of Acta Materialia Inc.

## 1. Introduction

Precipitation is a ubiquitous process that takes place in a solid or liquid solution when the composition of solute atoms exceeds its solubility limit as the temperature is lowered. In the case of solid-state precipitation, the microstructure of these precipitates on a nanometer or micron scale (i.e., the precipitate morphology, volume fraction, and spatial distributions) is a controlling factor in the mechanical properties of a material. The classic textbook example is the precipitation of nanoscale particles in Al with small additions of Cu, and the concomitant dramatic increase in mechanical strength. More than six decades of experimental study of this process has shown that the initial stage involves formation of plate-shape atomic clusters of Cu with a thickness of one (or very few) atomic layers, called GP zones, named after Guinier [1] and Preston [2] who first discovered them in 1938.

However, despite decades of extensive research and application of modern characterization tools, controversy still remains regarding the detailed atomic structure and composition of GP zones, as well as the kinetic mechanisms of their formation and growth (see e.g. [3–6]). Theoretical studies of the problem are also hampered by the time scale (seconds to days or longer) and spatial scale (from a few angstroms to tens of nanometers) of GP zone precipitation, which prevent the direct use of any individual computational approach such as first-principles calculations, molecular dynamics methods, or continuum mesoscale models. As a result, there is essentially no quantitative information available, either from theory or experiment, with regard to the temporal evolution kinetics of GP zone microstructures, i.e., the volume fraction, average size, and size distributions as a function of time. In this work, we integrate a number of state-of-the-art computational approaches to yield a solution to the problem:

---

* Corresponding author. Tel.: +1 814 863 8101; fax: +1 814 234 0965.
 *E-mail address:* lqc3@psu.edu (L.-Q. Chen).

first-principles total energy calculations, the mixed-space cluster expansion [7,8] and Monte Carlo simulations [9,10]. Our main objectives are (1) to predict the atomic structure, composition, and evolution of GP zones without a priori assumptions, (2) to elucidate the fundamental interactions leading to their formation, and (3) to deduce the quantitative transformation kinetics of GP zones.

## 2. Computational model

Central to this integrated computational approach is the development of a method capable of quickly and accurately producing energetics of $10^5$–$10^6$ atoms at finite temperatures. First-principles calculations, although quite accurate for metallic systems, are computationally limited to relatively small unit cells. Fortunately, a method already exists to obtain the energetics of million-atom cells at finite temperatures, with the accuracy of first-principles total energies, including both chemical and long-range strain energetics crucial to predicting the morphological evolutions in systems with significant atomic size mismatch: the mixed-space cluster expansion (MSCE) approach [7,8]. In this approach, we begin with a single underlying parent lattice (in the case of this paper, fcc), and define a configuration $\sigma$ by specifying the occupations of each of the lattice sites by an Al atom or a Cu atom. The variable $S_i = -1(+1)$ if the atom at site $i$ is Al (Cu). Within this context, the formation energy of any configuration with composition $Al_{1-x}Cu_x$ is written in terms of a generalized Ising-like model including long-ranged pair and many-body terms, as well as explicit inclusion of the coherency strain energy:

$$\Delta H(\sigma) = \sum_k J_{\text{pair}}(\mathbf{k})|S(\mathbf{k},\sigma)|^2 + \sum_f D_f J_f \overline{\prod}_f(\sigma)$$
$$+ \frac{1}{4x(1-x)} \sum_k \Delta E_{\text{CS}}^{\text{eq}}\left(\hat{\mathbf{k}},x\right)|S(\mathbf{k},\sigma)|^2. \quad (1)$$

Here, $f$ is a symmetry-distinct figure consisting of several lattice sites, $D_f$ is the number of figures per lattice site and the 'lattice-average product' $\overline{\prod}_f$ is defined as a product of the variables $S_i$, over all sites of the figure $f$ averaged over all symmetry equivalent figures of lattice sites. The mixed-space cluster expansion of Eq. (1) is separated into three parts. The first summation includes all pair figures with arbitrary separation. $J(\mathbf{k})$ and $S(\mathbf{k},\sigma)$ are lattice Fourier transforms of real-space pair interactions and spin-occupation variables. The second summation includes multibody (triplets, quadruplets, etc.) interactions, $J_f$ runs over symmetry non-equivalent clusters. The third summation involves $\Delta E_{\text{CS}}(\hat{\mathbf{k}},x)$, the 'coherency strain energy', defined as the energy required to maintain coherency between bulk Cu and Al along an

interface with orientation $\hat{\mathbf{k}}$. The pair and multibody interactions, $J(\mathbf{k})$ and $J_f$, may be obtained by fitting Eq. (1) to a series of first-principles-calculated total energies for ordered arrangements of Al and Cu atoms, and the coherency strain energies are calculated by deforming the bulk elements (Al and Cu) from their equilibrium lattice constants to a common lattice constant perpendicular to $\hat{\mathbf{k}}$. The coherency strain energy is a function of composition $x$ and direction $\hat{\mathbf{k}}$ only, but does not include information about the strength of chemical interactions between Al and Cu.

The mixed-space cluster expansion Hamiltonian for face-centered-cubic (fcc) Al–Cu was constructed [11] using full-potential linearized augmented plane-wave (FLAPW) total energy calculations. All FLAPW calculations employed the local density approximation (LDA) and were fully relaxed to their energy-minimizing geometry with respect to volume, unit-cell vector lengths and cell internal coordinates. Total energies of 41 ordered compounds were used to fit the values of the effective interaction energies. These ordered compounds included a wide variety of local configurations and ordered structure types: short-period superlattices for a variety of orientations (e.g., [100], [111], and [110]), special quasi-random structures (ordered structures which mimic the random alloy), dilute supercells of isolated {100} monolayers and bilayers, an isolated substitutional Cu impurity, and other structures. The MSCE Hamiltonian fit to these structures consisted of 50 pair interactions, five triplet, and four quadruplet interactions in addition to the reciprocal-space anharmonic coherency strain energetics. This complex mixed-space Hamiltonian was then used in Monte Carlo simulations. For more details of the FLAPW calculations and the MSCE fit of the Al–Cu energetics, we refer the reader to [11]. We note that the MSCE combined with thermodynamic Monte Carlo simulations have been used to predict the equilibrium precipitate shapes in several Al alloys [9,12,13]. However, we wish to go beyond equilibrium thermodynamics; hence we combine our mixed-space cluster expansion with a dynamic method using Monte Carlo (MC) simulations with Kawasaki spin-exchange dynamics [12,13].

## 3. Results and discussions

For our Monte Carlo simulations, we use three different compositions, i.e., Al–1.0at.%Cu, Al–1.5at.%Cu and Al–2.0at.%Cu at temperatures $T = 273$, 373 and 473 K, respectively. The MC simulation cell consists of $N^3$ lattice sites with fixed compositions and periodic boundary conditions. Most results shown are taken from simulations with $N = 64$ (262,144 atoms), but we also performed a relatively short-time simulation with one million atoms ($N = 100$) to confirm that our results with

$N = 64$ are representative of those of larger systems at the early stage of the precipitation process. The time step in the Monte Carlo simulation is converted to real time based on a crude approximate relation between successful atom jump frequency, $1/\tau_0$, and the experimental diffusion coefficient $D_{\exp}(T)$ via $\tau_0(T) = a_{nn}^2/D_{\exp}(T)$, where $a_{nn}$ is the average nearest-neighbor distance between atoms [9]. We find that $\tau_0(T) \approx 5.2 \times 10^{10}$, 8000, and 0.9 s for $T = 273$, 373, and 473 K, respectively.

In Fig. 1, we demonstrate our approach by showing the concurrent nucleation, growth, and coarsening processes of coherent Cu precipitation in an Al matrix within a single, predictive, first-principles-based methodology. The perspective direction of view in this figure is [1 0 0]. From the figure, it is apparent that starting with an initially random distribution of Cu, precipitates appear and grow as individual single atomic layers of Cu along the {1 0 0} planes of the fcc lattice of Al atoms. Our simulations show that the GP zones form as plates of one monolayer thick along the {0 0 1} planes and consist of 100% Cu atoms.

We wish to compare our predicted morphologies with those experimentally observed. In Fig. 2, a snapshot of an atomic distribution from our Monte Carlo simulation is compared to a recent observation of GP zone nanoscale structure [5,6] in Al–Cu by atomic-resolution high-angle annular detector dark-field scanning transmission electron microscopy. The morphology of the experimentally observed GP zones, a monolayer thickness with the habit planes along the (0 0 1) directions, is precisely the same as predicted from our first-principles MSCE method, giving us confidence in the accuracy of our approach. Although the atomic-scale detail of the zones, such as the composition of Cu within the plates, is very difficult to determine experimentally, our calculations clearly demonstrate that the GP zones consist of pure Cu atoms, thus resolving one of the controversies with regard to the composition of GP zones. Based on equilibrium MC simulations, the GP zone solvus temperature obtained from the first-principles Al–Cu cluster expansion is about 50–100 K higher than the corresponding experimentally determined solvus temperature [11]; thus, we compare a simulation at 373 K with an experimental aging at 300 K in Fig. 2. We also note that the aging time for the experimental picture is shorter than that from the simulation (Fig. 2). We account for this difference due to the quenched-in non-equilibrium vacancies, thus higher atomic diffusivity in the experiment.

Following the classical work of Khachaturyan [14], the shape of a precipitate is controlled by two competing factors: While the interfacial or chemical energy typically leads to a compact shape, the strain leads to a flattening along the elastically soft direction of the precipitate. The former corresponds to the Wulff construction. Our MSCE Hamiltonian allows for a separation into these two characteristic energy contributions
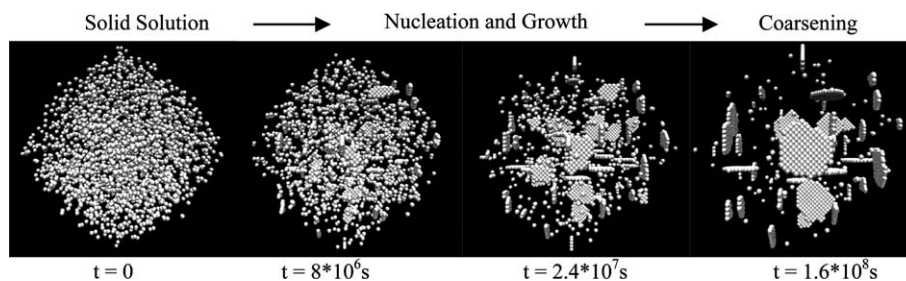


Fig. 1. First-principles MSCE calculated evolution of GP zones with Al–1.0at.%Cu at $T = 373$ K Only Cu atoms are shown, and from the perspective view, it can be seen that precipitates form three variants of monolayer (1 0 0) plates consisting of pure Cu. Simulation times are shown in seconds.
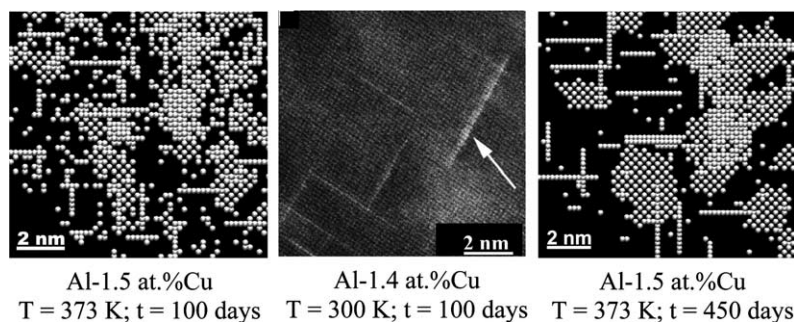


Fig. 2. Comparison of predicted and observed GP zones nanostructures in Al–Cu. The observed GP zone image is taken from [6]. The calculated structure represents a snapshot from a Monte Carlo simulation; only Cu atoms are shown.

by eliminating the elastic interactions in the total Hamiltonian. We do not observe any plate-like precipitates even after a long simulation, and therefore we conclude that the anisotropic elastic interactions arising from the atomic size mismatch between Al and Cu atoms are indeed responsible for the GP zone habit orientation along {1 0 0} and for their one atomic layer thickness rather than the interfacial energy anisotropy. We note that for a nucleation and growth study of the type we have performed, a necessary prerequisite of the model is that the equilibrium precipitate shape must first be correct in order to have any chance of getting insight into the evolution kinetics. Our first-principles MSCE method includes both interfacial and strain energetics, and has been proven to provide the accurate equilibrium precipitate shapes in the case of GP zones in Al–Cu [11].

From our first-principles MSCE approach, we go beyond qualitative comparison with experiment and obtain quantitatively the kinetics of GP zone precipitation. We analyzed, from the Monte Carlo simulations, the time-dependence of the number of GP zones, their sizes and size distributions, and volume fraction. In this paper, a GP zone is defined when three nearest-neighbor bonds of a Cu atom are between Cu atoms, and we focus our analysis on the initial stage of precipitation before significant coarsening takes place. We first examined the atomic configurations during the initial stage of precipitation to determine whether the precipitation process follows the classical, homogeneous nucleation and growth mechanism or the spinodal mechanism. We observed the formation and growth of Cu clusters as well as the disappearance of very small clusters, consistent with the classical nucleation and growth mechanism. We also ascertained the time-dependence of the volume fraction (defined as the fraction of Cu atoms in GP zones), as well as the number, shapes, and sizes of each of the zones. The number of GP zones as a function of time for the case of 373 K and 1.0 at.% Cu is shown in Fig. 3. This figure yields interesting information regarding the nucleation behavior of GP zones:

If all the nuclei were formed at once, the number of GP zone would either be constant or decrease as a function of time. Hence, the increase in the number of GP zones at the early stages indicates continuous nucleation. However, the rate of nucleation is not constant, otherwise the number of GP zones would follow a straight line as a function of time. The nucleation rate shows a slight increase at early times and then decreases as a function of time (Fig. 3). The number of GP zones decreases at later times, indicating that the system is at the coarsening stage at which larger GP zones grow and smaller ones disappear.

Fig. 4 shows the normalized volume fraction as a function of time for 373 K and Al–1.0at.%Cu. We analyzed the results using the classic theory for the phase transformation kinetics, i.e., the Johnson, Mehl, and Avrami theory (JMA) [15–17], which can be summarized by

$$f' = 1 - \exp[-kt^n], \qquad (2)$$

where $f'$ is the normalized volume fraction of GP zones as a function of time ($t$), $f'(t) = f(t)/f_{eq}$, $f(t)$ is the instantaneous volume fraction of GP zones at time $t$ and $f_{eq}$ the equilibrium ($t \rightarrow \infty$) volume fraction determined by thermodynamics. $n$ is the transformation exponent that may depend on conditions such as precipitate morphology, the dimensionality of the system, as well as the time-dependence of nucleation rate. We have fit our results in Fig. 4 to an equation of the form in Eq. (1). The JMA functional form provides a good description for the nucleation and growth stage (see the inset in Fig. 4 which represents the volume fraction transformed as a function of time during the nucleation and growth stage).

We wish to understand the physics underlying the growth behavior of plate-shaped particles in Fig. 4. To
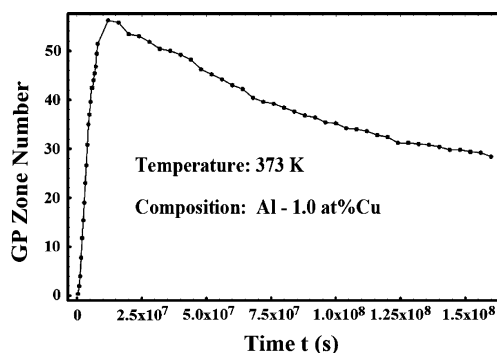


Fig. 3. First-principles MSCE calculated number of GP zones vs. time $t$ (s). The shape of the curve is consistent with a continuous nucleation of zones, but with a decreasing rate.
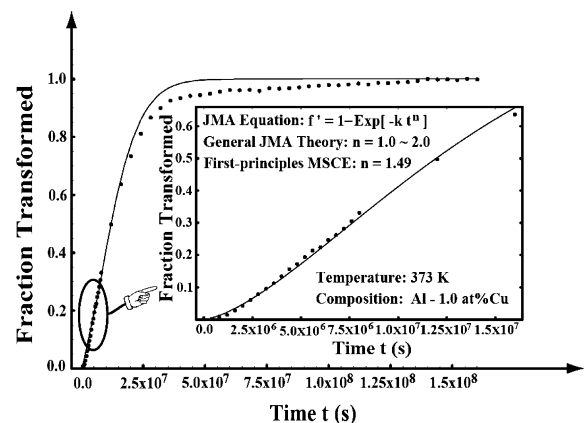


Fig. 4. First-principles MSCE calculated volume fraction of GP zones (dotted line: first-principles MSCE; solid line: generalized JMA theory). Note that the transformation exponent is $n \sim 1.5$, intermediate between the limiting values corresponding to a constant nucleation rate ($n = 2$) or a fixed number of nucleation sites ($n = 1$).

that end, we have adapted the JMA theory to our situation of plate-shaped GP zones: Consistent with our calculated results above, we assume in our derivation that the thickness of the GP zones is constant during nucleation and growth. In order to derive a growth expression, we must also know the dependence of the particle radius $r(t)$ on time during the growth phase. Based on the dimensional argument of Zener [18], the dependence should follow $\bar{r}(t) \propto \sqrt{t}$, which has been experimentally verified by Czeczor et al. [19] and Hardy [20] for GP zones in Al–Cu. To elucidate this dependence from our methodology, we have performed MC simulations with an initial configuration of a single GP zone containing 21 Cu atoms placed in a solid solution. From this simulation, we extract the growth law for a single GP zone, finding $\bar{r}(t) \propto \sqrt{t}$, consistent with experiment. Using this information with the above assumptions, we have derived JMA expressions [17] in two limiting cases: (1) for the case of constant nucleation rate, $I_s$, during growth and (2) for the case of a fixed number of nucleation sites, with all GP zones nucleated at time $t = 0$ and the nucleation rate dropping zero at $t > 0$. For the first case, we find:

$$f' = 1 - \exp\left[-\left\{(c^\beta - c^\alpha)/(c^o - c^\alpha)\right\}\frac{\pi(\alpha_2)^2 dD I_s t^2}{2}\right]$$
$$= 1 - \exp[-k_1 t^2],$$

where $c^o$, $c^\alpha$ and $c^\beta$ are the overall composition, equilibrium composition of the fcc matrix, and the equilibrium composition of the GP zones, respectively. $D$ is the Cu diffusion coefficient in the Al fcc matrix, $d$ the thickness of GP zones and $\alpha_2$ geometrical growth constant. For the second case, we find:

$$f' = 1 - \exp\left[-\left\{(c^\beta - c^\alpha)/(c^o - c^\alpha)\right\}\pi(\alpha_2)^2 dD N_v t\right]$$
$$= 1 - \exp[-k_2 t], \tag{4}$$

where $N_v$ is the total number of preexisting nucleation sites per unit volume. Therefore, the general transformation kinetics for GP zone formation can be written as [17] $f' = 1 - \exp[-kt^n]$ with $n$ in the range $n = 1$–$2$ for diffusion-controlled nucleation and growth of plate-shaped particles with a fixed plate thickness.

We have extracted values of the transformation exponent, $n$, from our first-principles MSCE calculations for different compositions and temperatures. These values for the transformation exponent obtained from the simulations indeed fall between values for the two limiting cases, 1.0 and 2.0. For Al–1.0at.%Cu, Al–1.5at.%Cu and Al–2.0at.%Cu at $T = 373$ K, we find $n \sim 1.5$, 1.3, and 1.3, respectively. For Al–2.0at.%Cu at $T = 473$ K, we find $n \sim 1.5$. In our simulations, the Cu atoms are randomly distributed in Al matrix in the initial configuration, corresponding to a configuration quenched from high temperatures, so there are no nuclei present at time

0. Therefore, in our fits of Eq. (1) to the simulation data, we discarded the data corresponding to the first 50 Monte Carlo time steps ($4 \times 10^5$ s and 45 s for temperatures $T = 373$ K and $T = 473$ K, respectively) for each composition. The fact that the transformation exponent obtained from the simulation is less than 2.0 indicates that the nucleation rate is not a constant, but decreases as a function of time. This behavior is reasonable since the concentration of Cu in the matrix decreases as GP zones nucleate and grow, and therefore the supersaturation (the driving force for nucleation) also decreases. This explanation is also consistent with the time-dependence of the number of GP zones presented in Fig. 3. We have also numerically examined the sensitivity of the extracted values of $n$ to the end time for nucleation and growth. We consistently find a value of $n \sim 1.5 \pm 0.2$. Thus, somewhat surprisingly, the continuum JMA theory is applicable to the inherently atomistic problem of nanoscale precipitates in Al–Cu.

## 4. Conclusions

The morphological evolution and growth kinetics of GP zones in Al–Cu alloys are studied by a multiscale computational model integrating first-principles calculations, the mixed-space cluster expansion, and Monte Carlo simulations. Without fitting parameters, the model predicted the nucleation and growth of single atomic layers of Cu atoms along {1 0 0} planes of a fcc lattice of Al atoms. It is determined that the GP zones consist of 100%Cu atoms. It is demonstrated that it is indeed the strain-induced long-range interactions that are responsible for the plate-like shapes of GP zones. The precipitation kinetics is analyzed using the classical Johnson–Mehl–Avrami phase transformation theory and a transformation exponent of $\sim$1.5 is obtained.

## References

[1] Guinier. Nature 1938;142:669.
[2] Preston GD. Nature 1938;142:570.
[3] Ringer SP, Hono K. Mater Charact 2000;44(1–2):101.
[4] Gerold V. Scr Metall 1988;22:927.

[5] Konno TJ, Kawasaki M, Hiraga K. Philos Mag B 2001;81:1713.
[6] Konno TJ, Hiraga K, Kawasaki M. Scr Metall 2001;44:2303.
[7] Laks DB, Ferreira LG, Froyen S, Zunger A. Phys Rev B 1992;46:12587.
[8] Wolverton C, Zunger A. Phys Rev Lett 1995;75:3162.
[9] Müller S, Wang L-W, Zunger A. Modell Simul Mater Sci Eng 2002;10(2):131.
[10] Landau DP, Binder K. Guide to Monte Carlo simulations in statistical physics. Cambridge: Cambridge University Press; 2000.
[11] Wolverton C. Philos Mag Lett 1999;79(9):683.
[12] Wolverton C. Modell Simul Mater Sci Eng 2000;8(3):323.
[13] Müller S, Wolverton C, Wang L-W, Zunger A. Europhys Lett 2001;55:33.
[14] Khachaturyan AG. Theory of structural phase transformations. New York: Wiley; 1983.
[15] Johnson WA, Mehl KE. Trans Am Inst Min Met Eng 1939;195:416.
[16] Avrami M. J Chem Phys 1939;7:1103;
Avrami M. J Chem Phys 1940;8:212;
Avrami M. J Chem Phys 1941;9:177.
[17] Christian JW. The theory of transformations in metals and alloys. 3rd ed. Oxford: Pergamon Press; 2002.
[18] Zener C. J Appl Phys 1949;20:950.
[19] Czeczor S, Löchte L, Gottstein G, Staron P, Kampmann R. Phys Stat Sol (a) 2000;182:631.
[20] Hardy HK. J Inst Metals 1951;79:321.